Realization and Implementation of Adaptive Control for Permanent Magnet Synchronous Motor on an Electric Vehicle

Yi-Hsien Chiang [1], Ya-Wen Shih, and Shih-Wei Hung
[1]*Mechanical and system Laboratories, Industrial Technology Research Institute, Bldg. 58, Chung Hsing Rd., Section 4, Chutung, Hsinchu, Taiwan, acloud@itri.org.tw*

Abstract

This paper presents an adaptive control approach implemented on Permanent Magnet Synchronous Motor (PMSM) drives to account for the uncertainties of the model parameters. A Hall-effect sensor is utilized as the incremental measurement to estimate the angular speed and position instead of high cost encoder or resolver with the consideration of reliability, particularly in propulsion system of Hybrid Electric Vehicles (HEV). The paper mainly addresses the problem of parametric divergence of the PMSM adaptive control scheme, induced by the current ripples with the multiples of electric rotational frequency. Unfortunately, any methodology for the ripple reduction is not suitable in this case unless the undesired harmonic signals can be eliminated entirely. To tackle the vital obstacle for the realization of the adaptive control, a slow adaptation law by filtering out the higher harmonics from the currents on d-q rotor frame is proposed. The experimental results show that the proposed novel control scheme can make the PMSM adaptive current loop control work properly.

Keywords: Permanent magnet synchronous motor, adaptive control, ripple, electric vehicle

1 Introduction

Hybrid Electric vehicles (HEV) have been regarded as one of solutions to mitigate energy and environmental problems nowadays. In such the dynamic system, the partial power is delivered by electric motor in traction mode and kinetic energy is recuperated while braking. Thus Permanent magnet synchronous motors (PMSM) have been widely used in propulsion system of the HEVs due to their high efficiency, low noise, compact size, and comparatively high traction power by comparing to other types of motors. Furthermore, it achieves the merit by generating rotor magnetic flux with the rotor magnet entails knowing the rotor position to implement field-oriented control theory.

Due to the reliability issue of high resolution encoders requested to operate in harsh environment of HEVs, the sensorless control approaches have been proposed to reduce the system cost and avoid the risk of failure of the sensors while the vehicle is cruising at high speed. Nevertheless, the PMSM control systems proposed in [2], [3], [5], [8], [10], [12], [13], [14], [17], and [19] cannot be used to start the motor from standstill because of low SN ratio and model inaccuracy. Therefore, some literatures proposed some practical methods for the initial rotor position estimation [1], [16], [18].

Adaptive control approaches has been employed to account for the variations or uncertainties of the model parameters [6], [11], [21]. Furthermore, [20] proposed observer-based adaptive control algorithm to achieve the speed regulation with initial rotor position uncertainty. However, the PMSM model given in the adaptive control systems mentioned above generates a sinusoidal back-EMF waveform in 3-phases. In practice, the

trapezoid back-EMF waveform commonly found in the PMSM systems resulted from its inherent higher harmonics so that the undesired current ripples could occur. Such the harmonics are hardly modelled and cannot be completely eliminated but mitigated to some lower level [4], [7], [9], [15]. On the other hand, the adaptation law is usually computed by numerical integration of the product of the measurable current and voltage signals, the irremovable higher frequency ripples could cause the parametric divergence problem in the adaptive control systems.

For the development of the sensorless PMSM drives for EV in this paper, the cheap and reliable Hall-effect sensor that divides the electric rotational plane into 6 sectors is adopted to act as an incremental encoder with the uncertainty of $\pm 30^{o}$ on each sector. Furthermore, the propulsion drives of the EVs usually operate over a wide speed range and induce the heat problem as well. Those factors are likely to cause the motor parameters to vary with their operating circumstances. To handle the PMSM systems subject to the above problems, a direct adaptive control algorithm is employed to achieve the current loop control. However, it is shown that the adaptation law cannot work in the case where the higher harmonics are carried in the currents. A filtering process for eliminating the current ripples on the particular frequencies is conceived to make the devised controller practicable on the PMSMs as main contribution of this paper.

This paper is organized as follows. In Section 2, the sensorless PMSM drive with unknown initial rotor position is formulated into the control problem with the parametric uncertainties. In Section 3, the direct adaptive control law is devised by means of Lyapunov stability theory for assuring the stability of the current loop control system. The filtering process is proposed to implement the adaptive control scheme to bear the currents with the higher harmonics. In Section 4, the experimental results are presented to demonstrate the effectiveness of the proposed adaptive control scheme. Finally, the conclusions are given.

2 Mathematical Model of PMSM

In our PMSM control system, an integrated circuit of the Hall sensors is mounted to the motor to act as an incremental encoder that uniformly divides the electric rotational plane into 6 sectors as shown in Figure 1. At startup, the Hall sensor barely indicates at which sector the rotor axis locates. It can be seen that there still exists the uncertainty of $\pm 30^{o}$ to align with its actual position. The average electric rotational speed can be estimated though the count of timestamp within one sector and updated on each sector shift. Assume the initial electric position is θ_0 ccw relative to the beginning angle of any sector at motor startup. The rotor position can be estimated as

$$\theta = \theta_0 + \bar{\omega}_e(i-1)\sum_i \Delta t \tag{1}$$

where θ is rotor position, $\bar{\omega}_e(i-1)$ is average electric speed at previous sector $i-1$, and Δt is time step.

It is known that a typical PMSM dynamic system can be described in the actual synchronous d-q reference frame as

$$\begin{bmatrix} L_d & 0 \\ 0 & L_q \end{bmatrix}\begin{bmatrix} \dot{i}_d \\ \dot{i}_q \end{bmatrix} + \begin{bmatrix} R & -\omega_e L_q \\ \omega_e L_d & R \end{bmatrix}\begin{bmatrix} i_d \\ i_q \end{bmatrix} = \begin{bmatrix} u_d \\ u_q \end{bmatrix} - \begin{bmatrix} 0 \\ \omega_e \lambda \end{bmatrix} \tag{2}$$

where i_d, i_q, u_d, u_q, L_d, and L_q are stator currents, voltages, and inductances, respectively, in the d-q synchronous frame, R is stator resistance, λ is flux-linkage of the rotor magnet, and ω_e is electric rotational speed. In our case that (2) is not valid for the unknown θ_0. To see that, introduce a transformation matrix

$$\mathbf{T}(\theta_0) = \begin{bmatrix} \cos\theta_0 & \sin\theta_0 \\ -\sin\theta_0 & \cos\theta_0 \end{bmatrix} \tag{3}$$

such that

$$\mathbf{V}_{dq}^{a} = \mathbf{T}(\theta_0)\mathbf{V}_{dq}^{s} \tag{4}$$

where $\mathbf{V}_{dq}^{a}$ and $\mathbf{V}_{dq}^{s}$ denote state vectors in the actual and stator frame, respectively. According to (3) and (4), (2) can be rewritten as

$$\mathbf{L}_1(\theta_0)\begin{bmatrix} \dot{i}_d \\ \dot{i}_q \end{bmatrix} = -\left(\mathbf{R} + \omega_e \mathbf{L}_2(\theta_0)\right)\begin{bmatrix} i_d \\ i_q \end{bmatrix} - \omega_e \mathbf{E}_b(\theta_0) + \begin{bmatrix} u_d \\ u_q \end{bmatrix} \tag{5}$$

where

$$\mathbf{L}_1(\theta_0)=\mathbf{T}^{-1}(\theta_0)\begin{bmatrix}L_d & 0\\ 0 & L_q\end{bmatrix}\mathbf{T}(\theta_0)$$
$$=\begin{bmatrix}L_d\cos^2\theta_0+L_q\sin^2\theta_0 & (L_d-L_q)\sin\theta_0\cos\theta_0\\ (L_d-L_q)\sin\theta_0\cos\theta_0 & L_d\sin^2\theta_0+L_q\cos^2\theta_0\end{bmatrix},$$

$$\mathbf{R}=\mathbf{T}^{-1}(\theta_0)\begin{bmatrix}R & 0\\ 0 & R\end{bmatrix}\mathbf{T}(\theta_0)=R\mathbf{I}_2,$$

$$\mathbf{L}_2(\theta_0)=\mathbf{T}^{-1}(\theta_0)\begin{bmatrix}0 & -L_q\\ L_d & 0\end{bmatrix}\mathbf{T}(\theta_0)$$
$$=\begin{bmatrix}(L_q-L_d)\sin\theta_0\cos\theta_0 & -L_d\sin^2\theta_0-L_q\cos^2\theta_0\\ L_d\cos^2\theta_0+L_q\sin^2\theta_0 & (L_d-L_q)\sin\theta_0\cos\theta_0\end{bmatrix},$$

$$\mathbf{E}_b(\theta_0)=\mathbf{T}^{-1}(\theta_0)\mathbf{E}_b=\mathbf{T}^{-1}(\theta_0)\begin{bmatrix}0\\ \lambda\end{bmatrix}=\lambda\begin{bmatrix}-\sin\theta_0\\ \cos\theta_0\end{bmatrix}.$$

Consequently, the PMSM model with the initial uncertain position θ_0 can be also formulated in first ODE form as

$$\begin{bmatrix}\dot{i}_d\\ \dot{i}_q\end{bmatrix}=-\mathbf{L}_1^{-1}(\theta_0)\left(\mathbf{R}+\omega_e\mathbf{L}_2(\theta_0)\right)\begin{bmatrix}i_d\\ i_q\end{bmatrix}$$
$$-\omega_e\mathbf{L}_1^{-1}(\theta_0)\mathbf{E}_b(\theta_0)+\mathbf{L}_1^{-1}(\theta_0)\begin{bmatrix}u_d\\ u_q\end{bmatrix} \quad (6)$$

It can be found from (5) or (6) that the model parameters in terms of currents and voltages are all coupled with nonlinear functions with respect to θ_0. It is worth noting that (5) is a general model for salient and non-salient rotor. In particular, the uncertainty θ_0 only contributes to back-EMF term for the non-salient rotor case where $L_d=L_q=L$.

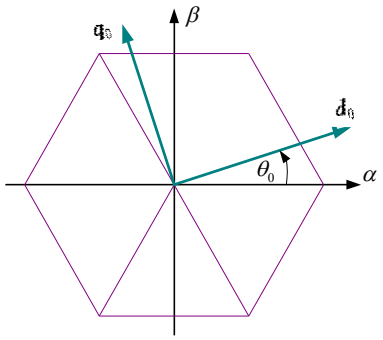

Figure 1: Initial position of d-q axis of PMSM referring to the fixed frame and the plane divided by Hall-effect sensor

3 Adaptive Controller Design and Modification

The PMSM used to be propulsion drive of EVs usually attempts to operate on the wide speed range. In addition, the torque command on the motor is altered frequently to respond any travelling circumstances, making the heat problem generated from the stator very complicated to be handled. It also causes the variations of the electric motor parameters as well as degrades the performance under the model-based control approaches. Thus the adaptive or robust control is much accepted in such an application.

In our PMSM system, we address a current loop control problem where the variations of the motor parameters and the initial position uncertainty are taken into account. Recall that the position uncertainty is formulated to couple with the motor parameters to yield complex ones that can be regarded as new model parameters so as to employ the direct adaptive control algorithm. It follows the theorem as below.

Theorem

For the PMSM current loop control system described in (5) where the initial rotor position and the motor parameters are unknown, the current error for a given d-q current command can be attenuated to zero by the voltages of the d-q frame with the control input

$$u=\begin{bmatrix}u_d\\ u_q\end{bmatrix}=\hat{\mathbf{L}}_1(\theta_0)\left(\mathbf{F}_2\hat{\boldsymbol{\varphi}}_2+\mathbf{K}\mathbf{z}\right) \quad (7)$$

together with the adaptation law

$$\dot{\hat{\boldsymbol{\varphi}}}^T=\mathbf{z}^T\mathbf{F}\boldsymbol{\Lambda} \quad (8)$$

where $\mathbf{z}\begin{bmatrix}z_d\\ z_q\end{bmatrix}=\begin{bmatrix}i_{d\_\mathrm{ref}}-i_d\\ i_{q\_\mathrm{ref}}-i_q\end{bmatrix}$ denotes current error vector, i_{d_ref} and i_{q_ref} are current command in the d-q rotor frame, respectively, and

$$\mathbf{F}=\begin{bmatrix}\mathbf{F}_1 & \mathbf{F}_2\end{bmatrix},$$
$$\mathbf{F}_1=\begin{bmatrix}-u_d & -u_q & 0 & 0\\ 0 & 0 & -u_d & -u_q\end{bmatrix},$$
$$\mathbf{F}_2=\begin{bmatrix}i_d & i_q & 0 & 0 & \omega_e i_d & \omega_e i_q & 0 & 0\\ 0 & 0 & i_d & i_q & 0 & 0 & \omega_e i_d & \omega_e i_q\end{bmatrix},$$
$$\begin{bmatrix}\omega_e & 0\\ 0 & \omega_e\end{bmatrix}$$
$$\boldsymbol{\varphi}=\begin{bmatrix}\boldsymbol{\varphi}_1^T & \boldsymbol{\varphi}_2^T\end{bmatrix}^T,$$

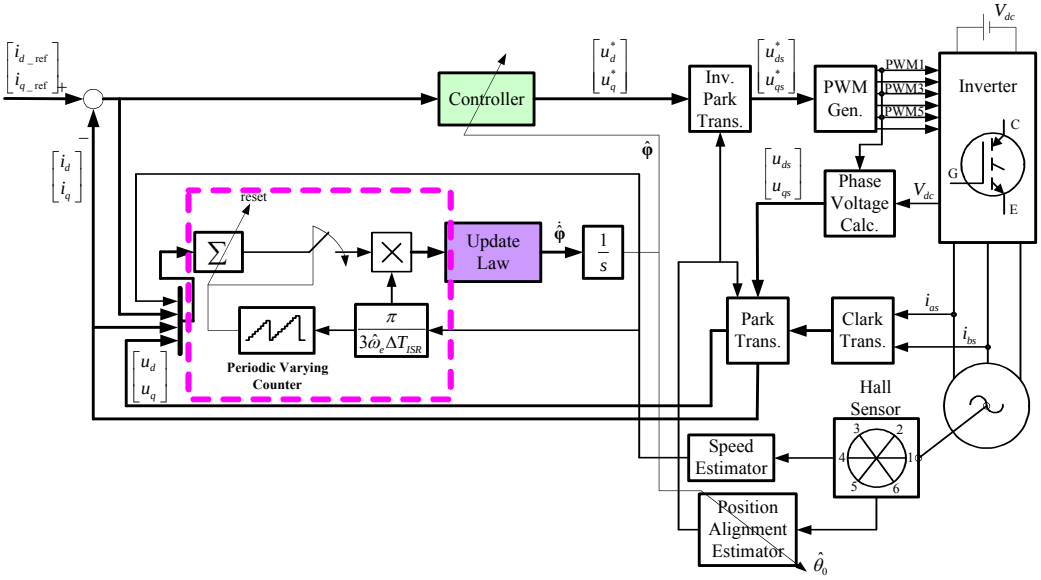

Figure 2: The proposed adaptive current control scheme with slow adaptation law

$$\boldsymbol{\varphi}_1^T = \begin{bmatrix} \mathbf{L}_1^{-1}(\theta_0)(1,1) & \mathbf{L}_1^{-1}(\theta_0)(1,2) \\ \mathbf{L}_1^{-1}(\theta_0)(2,1) & \mathbf{L}_1^{-1}(\theta_0)(2,2) \end{bmatrix},$$
$$\Box \begin{bmatrix} \phi(1,1) & \phi(1,2) & \phi(2,1) & \phi(2,2) \end{bmatrix}$$

$$\boldsymbol{\varphi}_2^T = \begin{bmatrix} \mathbf{L}_1^{-1}(\theta_0)\mathbf{R}(1,1) & \mathbf{L}_1^{-1}(\theta_0)\mathbf{R}(1,2) \\ \mathbf{L}_1^{-1}(\theta_0)\mathbf{R}(2,1) & \mathbf{L}_1^{-1}(\theta_0)\mathbf{R}(2,2) \\ \mathbf{L}_1^{-1}(\theta_0)\mathbf{L}_2(\theta_0)(1,1) & \mathbf{L}_1^{-1}(\theta_0)\mathbf{L}_2(\theta_0)(1,2) \\ \mathbf{L}_1^{-1}(\theta_0)\mathbf{L}_2(\theta_0)(2,1) & \mathbf{L}_1^{-1}(\theta_0)\mathbf{L}_2(\theta_0)(2,2) \\ \mathbf{L}_1^{-1}(\theta_0)\mathbf{E}_b(\theta_0)(1,1) & \mathbf{L}_1^{-1}(\theta_0)\mathbf{E}_b(\theta_0)(2,1) \end{bmatrix},$$
$$\Box \begin{bmatrix} \phi(2,1) & \phi(2,1) & \cdots & \phi(2,9) & \phi(2,10) \end{bmatrix}$$

$\mathbf{K}$ and $\boldsymbol{\Lambda}$ are positive-definite square matrices. Note that $\boldsymbol{\varphi}$ consists of all the uncertain model parameters in (6).

Proof – Consider the Lyapunov candidate function as

$$V = \frac{1}{2}\mathbf{z}^T\mathbf{z} + \frac{1}{2}\tilde{\boldsymbol{\varphi}}^T\boldsymbol{\Lambda}^{-1}\tilde{\boldsymbol{\varphi}}$$

where $\hat{\boldsymbol{\varphi}}$ is the estimation of $\boldsymbol{\varphi}$. $\tilde{\boldsymbol{\varphi}} = \boldsymbol{\varphi} - \hat{\boldsymbol{\varphi}}$ denotes the parametric error vector. According to (7), the derivative of $\mathbf{z}$ gives

$$\dot{\mathbf{z}} = \begin{bmatrix} \dot{z}_d \\ \dot{z}_q \end{bmatrix} = \begin{bmatrix} -\dot{i}_d \\ -\dot{i}_q \end{bmatrix}$$

$$= \mathbf{L}_1^{-1}(\theta_0)\left(\mathbf{R} + \omega_e\mathbf{L}_2(\theta_0)\right)\begin{bmatrix} i_d \\ i_q \end{bmatrix} + \omega_e\mathbf{L}_1^{-1}(\theta_0)\mathbf{E}_b(\theta_0) - \mathbf{L}_1^{-1}(\theta_0)\begin{bmatrix} u_d \\ u_q \end{bmatrix}$$
$$= \mathbf{F}_2\boldsymbol{\varphi}_2 - \mathbf{L}_1^{-1}(\theta_0)\begin{bmatrix} u_d \\ u_q \end{bmatrix}$$
$$= \mathbf{F}_2\boldsymbol{\varphi}_2 - \mathbf{L}_1^{-1}(\theta_0)\hat{\mathbf{L}}_1(\theta_0)\left(\mathbf{F}_2\hat{\boldsymbol{\varphi}}_2 + \mathbf{K}\mathbf{z}\right)$$
$$= \mathbf{F}_2\left(\tilde{\boldsymbol{\varphi}}_2 + \hat{\boldsymbol{\varphi}}_2\right) - \left(\hat{\mathbf{L}}_1^{-1}(\theta_0) + \tilde{\mathbf{L}}_1^{-1}(\theta_0)\right)\hat{\mathbf{L}}_1(\theta_0)\left(\mathbf{F}_2\hat{\boldsymbol{\varphi}}_2 + \mathbf{K}\mathbf{z}\right)$$
$$= -\mathbf{K}\mathbf{z} + \mathbf{F}_2\tilde{\boldsymbol{\varphi}}_2 - \tilde{\mathbf{L}}_1^{-1}(\theta_0)\begin{bmatrix} u_d \\ u_q \end{bmatrix}$$
$$= -\mathbf{K}\mathbf{z} + \mathbf{F}\tilde{\boldsymbol{\varphi}}$$

The derivative of V along the trajectory of the PMSM system (6) yields

$$\dot{V} = \mathbf{z}^T\dot{\mathbf{z}} - \dot{\tilde{\boldsymbol{\varphi}}}^T\boldsymbol{\Lambda}^{-1}\tilde{\boldsymbol{\varphi}}$$
$$= -\mathbf{K}\mathbf{z}^T\mathbf{z} + \mathbf{z}^T\mathbf{F}\tilde{\boldsymbol{\varphi}} - \dot{\hat{\boldsymbol{\varphi}}}^T\boldsymbol{\Lambda}^{-1}\tilde{\boldsymbol{\varphi}}$$
$$= -\mathbf{K}\mathbf{z}^T\mathbf{z} + \left(\mathbf{z}^T\mathbf{F} - \dot{\hat{\boldsymbol{\varphi}}}^T\boldsymbol{\Lambda}^{-1}\right)\tilde{\boldsymbol{\varphi}}$$
$$= -\mathbf{K}\mathbf{z}^T\mathbf{z} \le 0$$

provided that

$$\dot{\hat{\boldsymbol{\varphi}}}^T = \mathbf{z}^T\mathbf{F}\boldsymbol{\Lambda}.$$

□

It should be noted that the PMSM model given in (5) generates a sinusoidal back-EMF waveform in

3-phases since it is synchronous with d-q rotor frame. However, the trapezoid back-EMF waveform is commonly found in the PMSM systems. That is resulted from its inherent higher harmonics and undesired current ripples are likely to occur. Such the harmonics are hardly modelled and cannot be completely eliminated but mitigated to some lower level. Recall that the adaptive law in (8) is computed by numerical integration of the product of the measurable current and voltage signals, the irremovable higher frequency ripples could cause the parametric divergence in our control system. Unfortunately, this problem does happen to the implementation of the controller developed. In our preliminary experiments, it can be observed that there exits current ripples with the multiples of 6 times frequency of the electric speed by means of spectrum analysis on recorded data at startup. Then the current immediately surges over the limitation set for hardware protection after couple milliseconds. To tackle this, a filter process is conceived to take the mean values of the current and voltage for the maximum period of the ripples to eliminate those undesired terms. Hence, the parameters are updated slowly in the maximum period of the ripples depends on the rotational speed. The modified current loop adaptive control scheme is shown in Figure 2, in which the additional filter processing is encompassed with dashed line. Particularly, the estimated value of the initial rotor position can be evaluated as follows.

$$\frac{\hat{\mathbf{E}}_b\left(\hat{\theta}_0\right)(1,1)}{\hat{\mathbf{E}}_b\left(\hat{\theta}_0\right)(2,1)} = \begin{bmatrix} \hat{\phi}(1,1) & \hat{\phi}(1,2) \\ \hat{\phi}(2,1) & \hat{\phi}(2,2) \end{bmatrix}^{-1} \begin{bmatrix} \hat{\phi}(2,9) \\ \hat{\phi}(2,10) \end{bmatrix}, \quad (9)$$

$$\hat{\theta}_0 = -\tan^{-1}\left(\frac{\hat{\mathbf{E}}_b\left(\hat{\theta}_0\right)(1,1)}{\hat{\mathbf{E}}_b\left(\hat{\theta}_0\right)(2,1)}\right). \quad (10)$$

It can be used to update the rotor position in (1) as illustrated in Figure 2.

4 Experimental Results

The proposed control algorithm and scheme is implemented on a 15kW PM motor developed for a HEV. The PMSM drive is joined to a dynamometer that is able to provide maximum 20 kW capability for the traction and generation tests. In the configuration of test bench as shown in Figure 3, the motor control unit used to control the operation of PMSM is composed a DSP-based board for programming control algorithm and conventional 3-phase inverter circuit for DC to AC conversion.

In order to demonstrate the effectiveness of the proposed control system, the PMSM is driven at a constant speed 100 rpm. The current commands of d-q rotor synchronous frame are set to 0 and 10 A, respectively, viz $i_{d\_\mathrm{ref}} = 0$ and $i_{q\_\mathrm{ref}} = 10$. The motor parameters are initially set as $R = 0.005\ \Omega$, $L_d = 0.005$ H , $L_q = 0.003$ H , $\lambda = 0.015$ Wb , and $\theta_0 = 0^{\circ}$. The values of the model parameters used in the control process are listed on the rows of 'Startup' of Table 1. The experiments are run for two cases: one is based on the adaptive control law derived in (7) and (8) without taking the proposed filter process. The other one utilizes the same algorithm and the control scheme depicted in Figure 2. The results are shown in Figure 4-6 for the first case and Figure 7-10 for the second one.

In the first case, the currents on the d-q rotor frame and the variations of all the parameters were recorded separately in three tests due to limit of data stored on DSP Flash ROM as shown in Figure 4, 5 , and 6. It is shown that the currents on the d-q rotor frame in three tests all started to fluctuate widely at about 20 ms after the implementation of the PMSM control by seeing Figure 4(a)-(b), 5(a)-(b), 6(a)-(b). The fluctuations went on about 10 ms and the system was shut down because of the limitation of current on DC-link. Consequently, the figure 4(c)-(h), 5(c)-(h), and 6(c)-(d) show that the update law for the parameters also failed at the following time.

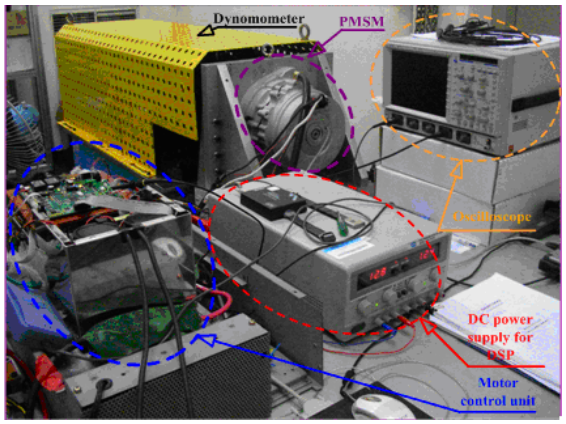

Figure 3: Configuration of test bench for PMSM drives

In the second experiment, the filter is added in the control scheme to take the mean values of the currents and voltages on the d-q rotor frame for one-sixth period of electric rotation at next adaptation. Obviously, the parameters are updated

Table 1: The model parametric values at control startup and steady-state

Parameter	$\phi(1,1)$	$\phi(1,2)$	$\phi(1,3)$	$\phi(1,4)$	$\phi(2,1)$	$\phi(2,2)$	$\phi(2,3)$	$\phi(2,4)$
Startup	200	0	0	333.33	1	0	0	1.67
Steadiness	199.4	-1.37	2.51	273.86	0.69	-0.15	-0.16	1.48
Parameter	$\phi(2,5)$	$\phi(2,6)$	$\phi(2,7)$	$\phi(2,8)$	$\phi(2,9)$	$\phi(2,10)$		
Startup	0	0	1.68	0	0	5		
Steadiness	-1.88	-0.86	0.77	-1.1	0.01	59.24		

more slowly since the adaptation rate is not according to interrupt time step but depends on the electric rotational speed. The control results are shown in Figure 7. Figure (a) and (c) are the currents, respectively, on the d- and q-axis of the rotor frame at the first 400 ms after the implementation of PMSM control. It is shown that the d- and q-axis currents are initially with some small ripples and q-axis current is pulled up slightly to the average positive value. The steady-state results are shown in (b) and (d) corresponding to d- and q-axis currents, respectively. It can be seen that their mean values are both regulated to the desired 0 and 10 A. However, the phenomenon of the carried ripples is getting little worse comparing to the initial currents. It is more apparent by checking their spectrum analysis as illustrated in Figure 8. The spectrum of magnitudes of d- and q-axis current errors are shown in Figure 8(a) and 8(b), respectively. Both currents are with the ripples at the multiples of frequency 40 Hz. It is also noted that there exists a ripple with the same frequency as the electric speed, viz. 40/6 Hz, carried by the d-axis current. Even though the unwanted ripples cannot be eliminated from the regulation of the currents, the adaptive control algorithm still works properly in our modified control scheme. The results of one of -3 phase currents displayed in an oscilloscope from control startup to steady-state are shown in Figure 9. The adaptation of the model parameters are shown in Figure 10. It can be observed that all the parameters are convergent within the first 15 seconds from the control startup in comparison with their steady-state values listed in Table 1.

5 Conclusions

It is known that the PMSM drives applied on the propulsion of EVs usually operate in the hot and moisture environment. The sensorless PMSMS control is imperative for such the applications. To this end, the PMSM is implemented by utilizing the Hall-effect sensor as the incremental encoder with the initial rotor position uncertainty of $\pm 30^{o}$ on each divided sector at the motor startup. The direct adaptive control approach is employed to achieve the current loop control objective and to account for the initial rotor position uncertainty as well as the variations of the model parameters. However, the higher harmonics of back EMF inherently induce the current ripples and result in the failure of the updated law of the model parameters. The concept of filtering the ripples out the currents is proposed to tackle this problem and the experimental results demonstrate the modified control system is able to work properly even though the current ripples cannot be removed.

The sensorless PMSM drives of electric vehicles based on the adaptive control algorithm can be enhanced by formulating higher back-EMF harmonics into the mathematical model. How to suppress the current ripples in this PMSM control system is our future work.

References

[1] A. Consoli, G. Scarcella, and A. Testa, “Sensorless control of AC motors at zero speed,” Proceedings of the IEEE International Symposium on Industrial Electronics, Vol. 1, pp. 373-379, 1999

[2] M. J. Corley and R. D. Lorenz, “Rotor position and velocity estimation for a salient-pole permanent magnet synchronous machine at standstill and high speeds,” IEEE Transaction on Industry Applications, Vol. 34, No. 4, pp. 784-789, 1998

[3] T. Furuhashi, S. Sangwongwanich, and S. Okuma, “A position-and-velocity sensorless control for brushless dc motors using an adaptive sliding mode observer,” IEEE Transactions on Industrial Electronics, Vol. 39, No. 2, pp. 89-95, 1992

[4] W. C. Gan and L. Qiu, “Torque and velocity ripple elimination of AC permanent magnet motor control systems using the internal model principle,” IEEE/ASME Transaction on Mechatronics, Vol. 9, No. 2, pp. 436-447, 2004.

[5] J. Gu, and Y. Zhang, Z. Wu, and J. Ying, "Rotor position and velocity estimation for PMSM based on sliding mode observer," IEEE International Conference on Power Electronics and Motion Control, Vol. 3, pp. 1351-1355, 2004

[6] Y. S. Han, J. S. Choi, and Y. S. Kim, "Sensorless PMSM drive with a sliding mode control based adaptive speed and stator resistance estimator," IEEE Transactions on Magnetics, Vol. 36, No. 5, pp. 3588-3591, 2000

[7] D. C. Hanselman, "Minimum torque ripple, maximum efficiency excitation of brushless permanent magnet motors," IEEE Transactions on Industrial Electronics, Vol. 41, No. 3, pp. 292-300, 1994

[8] A. A. Hassan and M. Azzam, "Robust control of a speed sensorless permanent magnet synchronous motor drive," International Conference on Technology and Automation, pp. 252-257, 2005

[9] J. Holtz and L. Springob, "Identification and compensation of torque ripple in high-precision permanent magnet motor drives," IEEE Transactions on Industrial Electronics, Vol. 43, No. 2, pp. 309-320, 1996

[10] A. B. Kulkarni and M. Ehsani, "A Novel position sensor elimination technique for the interior permanent-magnet synchronous motor drive," IEEE Transactions on Industry Applications, Vol. 28, No. 1, pp. 144-150, 1992

[11] L. Liu and D. A. Cartes, "Synchronisation based adaptive parameter identification for permanent magnet synchronous motors," IET Control Theory & Applications, Vol. 1, Issue 4, pp. 1015-1022, 2007

[12] N. Matsui, "Sensorless PM brushless dc motor drives, "IEEE Transactions on Industrial Electronics," Vol. 43, No. 2, pp. 300-308, 1996

[13] S. Morimoto, Y. Inoue, T. F. Weng, and M. Sanada, "Position sensorless PMSM drive system including square-wave operation at high-speed," IEEE International Conference on Industry Applications, pp. 676-682, 2007

[14] F. Parasiliti, R. Petrella, and M. Tursini, "Sensorless speed control of a PM synchronous motor based on sliding mode observer and extended Kalman filter," IEEE International Conference on Industry Applications, Vol. 1, pp. 533-540, 2001

[15] V. Petrović, R. Ortega, A. M. Stanković, and G. Tadmor, "Design and implementation of an adaptive controller for torque ripple minimization in PM synchronous motors," IEEE Transactions on Power Electronics, Vol. 15, No. 5, pp. 871-880, 2000

[16] M. Schroedl, "Sensorless control of ac machines at low speed and standstill based on the "INFORM" method," IEEE International Conference on Industry Applications, Vol. 1, pp. 270-277, 1996

[17] R. B. Sepe and J. Lang, "Real-time observer-based (adaptive) control of a permanent-magnet synchronous motor without mechanical sensors," IEEE Transactions on Industry Applications, Vol. 28, No. 6, pp. 1345-1352, 1992

[18] M. Tursini, R. Petrella, and F. Parasiliti, "Initial rotor position estimation method for PM motors," IEEE Transactions on Industry Applications, Vol. 39, No.6, pp. 1630-1640, 2003

[19] R. Wu and G. R. Slemon, "A permanent magnet motor drive without a shaft sensor," IEEE Transactions on Industry Applications, Vol. 27, No. 5, pp. 1005-1011, 1991

[20] . Yue, D. M. Vilathgamuwa, and K. J. Tseng, "Observer-based robust adaptive control of PMSM with initial rotor position uncertainty," IEEE Transaction on Industry Applications, Vol. 39, No. 3, pp. 645-656, 2003

[21] J. Zhou and Y. Wang, "Adaptive backstepping speed controller design for a permanent magnet synchronous motor," Proceedings of the IEE on Electric Power Applications, Vol. 149, No. 2, pp. 165-172, 2002

Authors

Yi-Hsien Chiang received the B.S. and M.S. degrees in the mechanical engineering in 1994 and 1996, respectively, and the Ph.D. degree in the electrical engineering in 2007 from the National Cheng Kung University, Taiwan.

He has been a researcher in Industrial Technology Research Institute, Taiwan since 2007. His current research interests include the motor control, energy management, and electric power systems on electric vehicles.

Ya-Wen Shih was born in Kaohsiung, Taiwan, R. O. C., in 1979. He received the B.S. degree in department of automatic control engineering from Feng Chia University, Taichung, Taiwan, in 2002 and received the M.S. degree in electrical engineering from Nation Cheng Kung University, Tainan, Taiwan, in 2004.

Since 2005, he has been an engineer in Industrial Technology Research Institute, Hsinchu, Taiwan. His research interests are motor control and system integration.

Shih-Wei Hung was born in Changhua, Taiwan, R. O. C., in 1980. He received the B.S. and M.S. degree in electrical engineering from Nation Taiwan University of Science and Technology, Taipei, Taiwan, in 2000 and 2004.

Since 2005, he has been an engineer in Industrial Technology Research Institute, Hsinchu, Taiwan. His research interests are motor design, control and system integration.

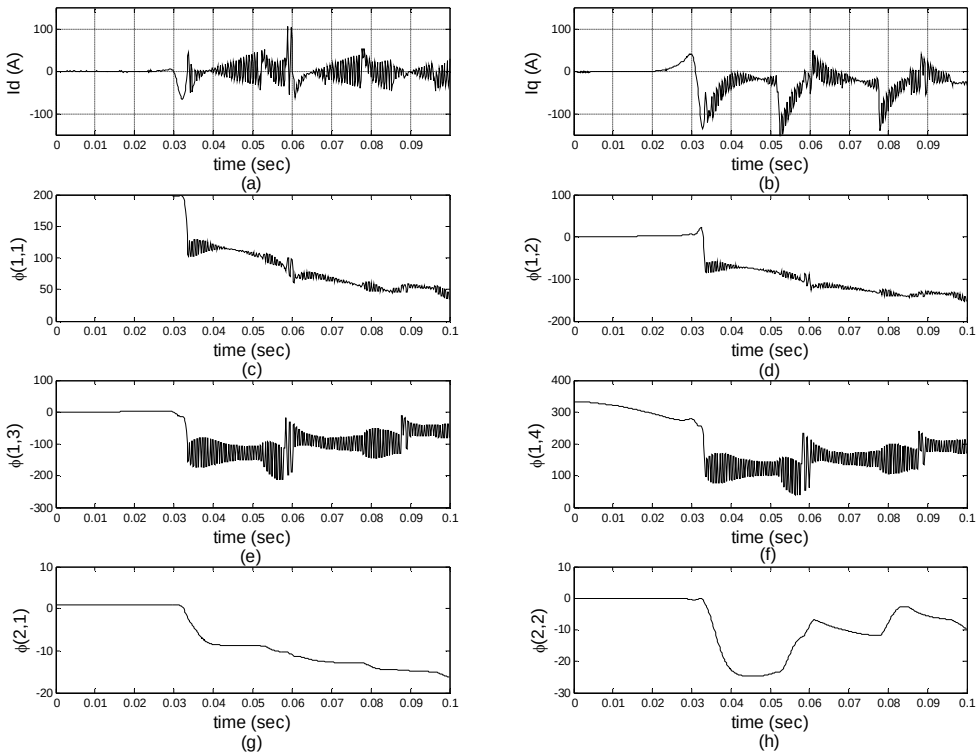

Figure 4: Experimental result (I): d-q currents and adaptation of model parameters $\phi(1,1) \sim \phi(2,2)$

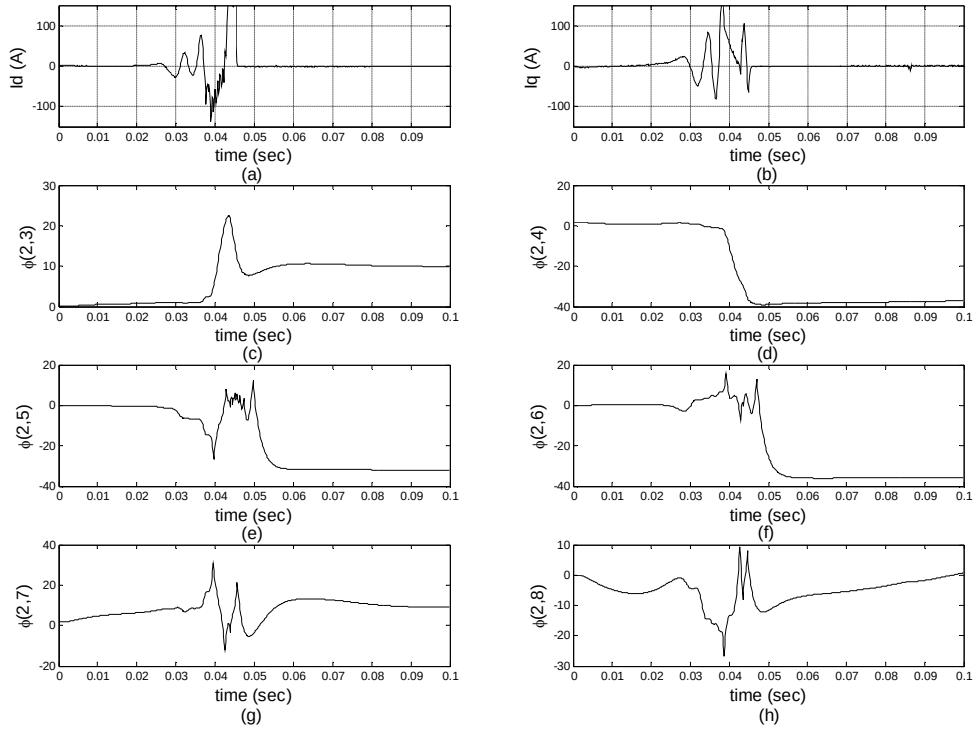

Figure 5: Experimental result (I): d-q currents and adaptation of model parameters $\phi(2,3) \sim \phi(2,8)$

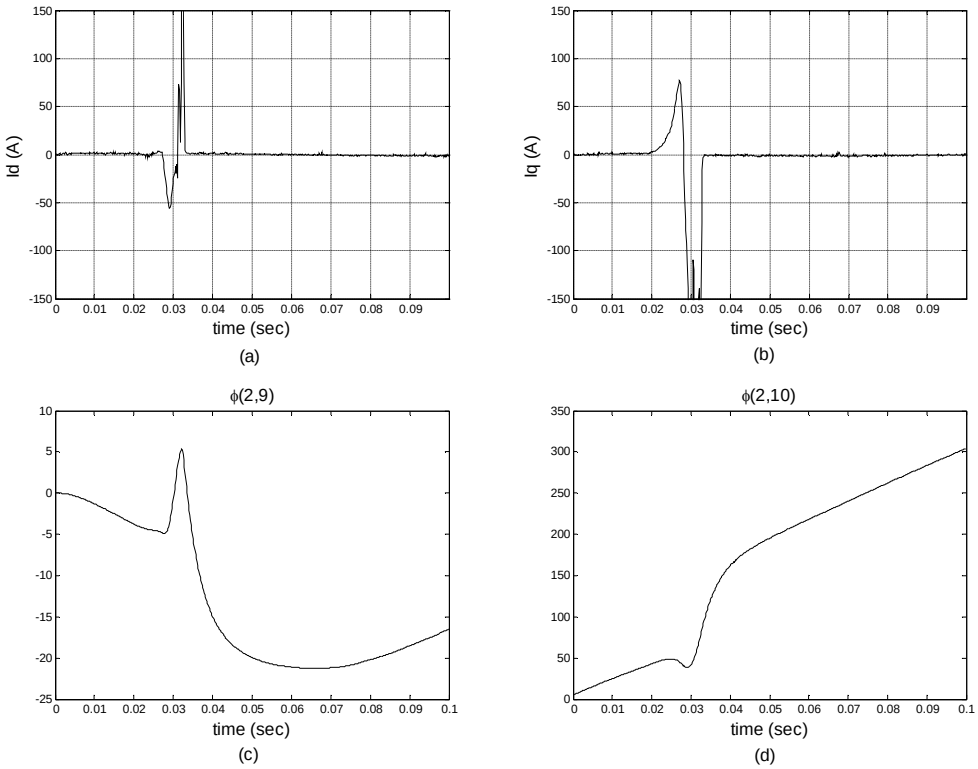

Figure 6: Experimental result (I): d-q currents and adaptation of model parameters $\phi(2,9)$ and $\phi(2,10)$

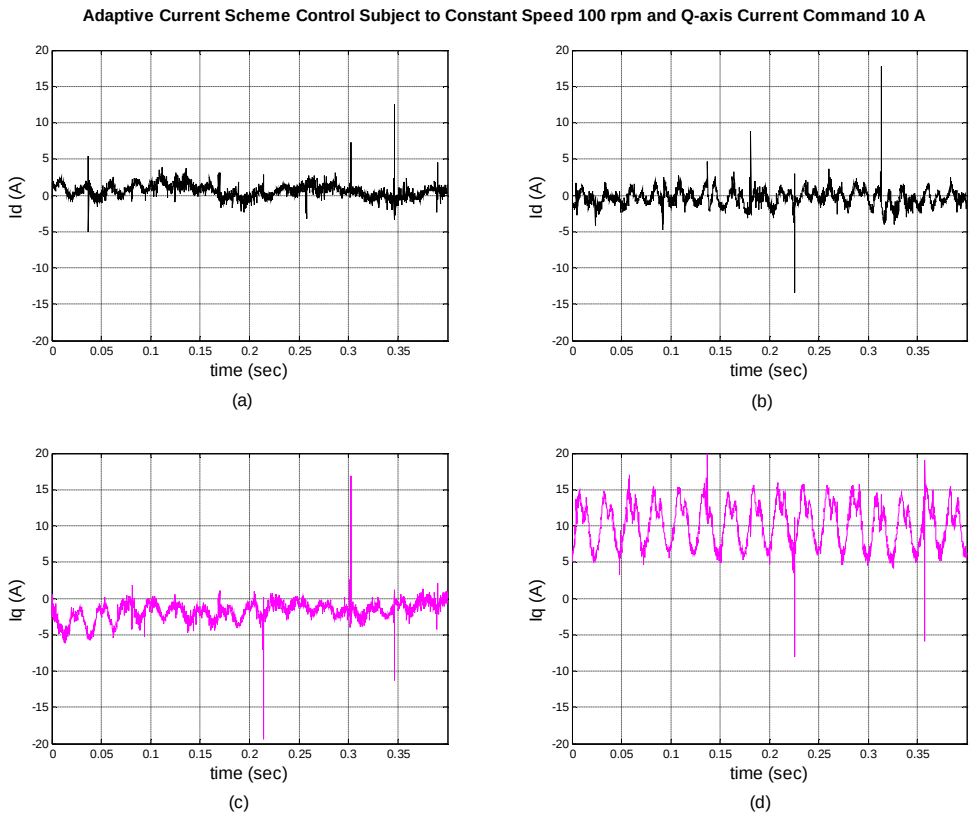

Figure 7: Experimental result (II): d-q currents at (a), (c) control startup and (b), (d) steady-state

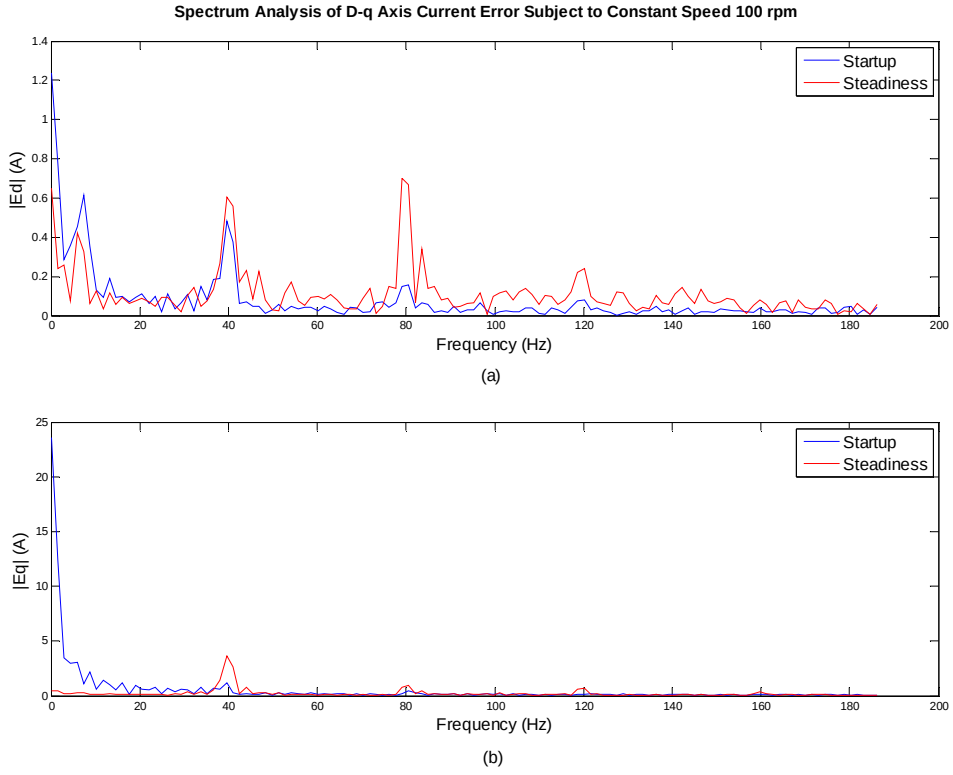

Figure 8: Experimental result (II): Spectrum analysis of d-q current errors at control startup and steady-state

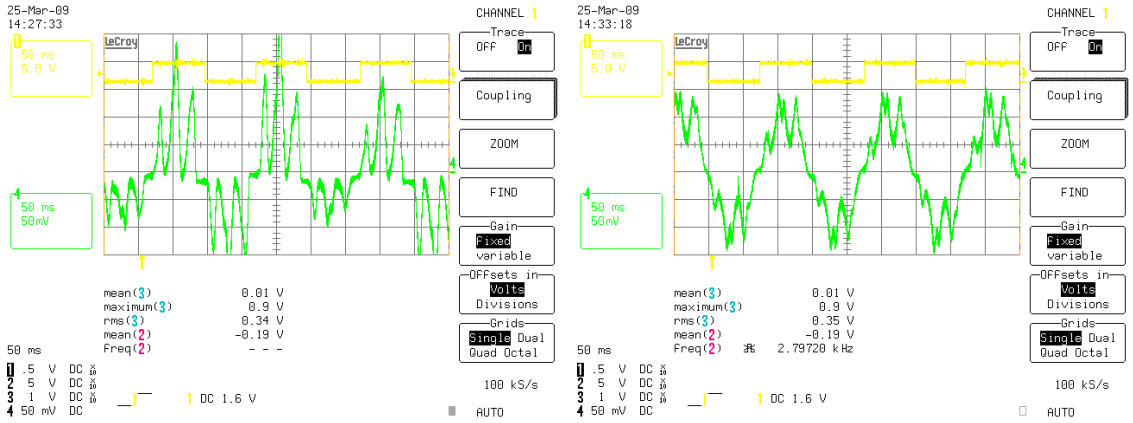

(a) (b)

Figure 9: One of 3-phase current waveforms at (a) control startup (b) steady-state

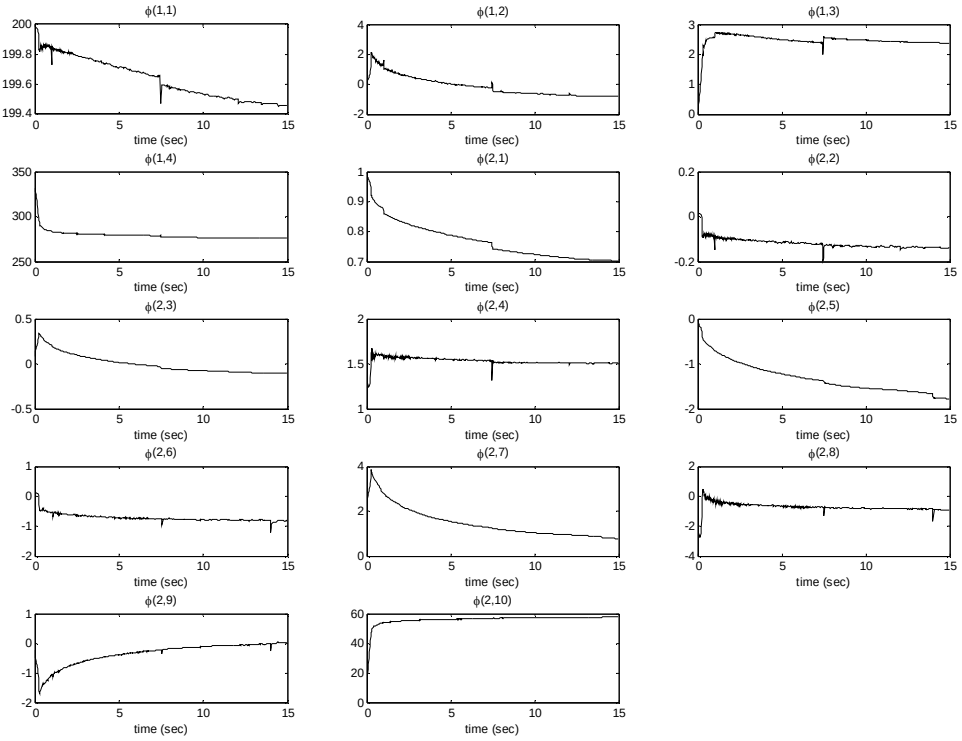

Figure 10: Experimental result (II): Adaptation of model parameters at control startup